Inorg. Chem. **2009**, *48*, 3720−3730

Cationic Clathrate I $Si_{46-x}P_xTe_y$ ($6.6(1) \leq y \leq 7.5(1)$, $x \leq 2y$): Crystal Structure, Homogeneity Range, and Physical Properties

J. V. Zaikina,[†,‡,§] K. A. Kovnir,[‡,§] U. Burkhardt,[‡] W. Schnelle,[‡] F. Haarmann,[‡] U. Schwarz,[‡] Yu. Grin,[‡] and A. V. Shevelkov*[,†]

Chemistry Department, Lomonosov Moscow State University, 119991 Moscow, Russia, and Max-Planck-Institut für Chemische Physik fester Stoffe, 01187 Dresden, Germany

Received December 15, 2008

A new cationic clathrate I $Si_{46-x}P_xTe_y$ ($6.6(1) \leq y \leq 7.5(1)$, $x \leq 2y$ at 1375 K) was synthesized from the elements and characterized by X-ray powder diffraction, thermal analysis, scanning electron microscopy, wavelength dispersive X-ray spectroscopy (WDXS), neutron powder diffraction, and ^{31}P NMR spectroscopy. The thermal behaviors of the magnetic susceptibility and resistivity were investigated as well. $Si_{46-x}P_xTe_y$ reveals a wide homogeneity range due to the presence of vacancies in the tellurium guest positions inside the smaller cage of the clathrate I structure. The vacancy ordering in the structure of $Si_{46-x}P_xTe_y$ causes the change of space group from $Pm\bar{3}n$ (ideal clathrate I) to $Pm\bar{3}$ accompanied by the redistribution of P and Si atoms over different framework positions. Neutron powder diffraction confirmed that P atoms preferably form a cage around the vacancy-containing tellurium guest position. Additionally, ^{31}P NMR spin−spin relaxation experiments revealed the presence of sites with different coordination of phosphorus atoms. Precise determination of the composition of $Si_{46-x}P_xTe_y$ by WDXS showed slight but noticeable deviation ($x \leq 2y$) of phosphorus content from the Zintl counting scheme ($x = 2y$). The compound is diamagnetic while resistivity measurements show activated behavior or that of heavily doped semiconductors. Thermal analysis revealed high stability of the investigated clathrate: $Si_{46-x}P_xTe_y$ melts incongruently at ∼1460 K in vacuum and is stable in air against oxidation up to 1295 K.

Introduction

Clathrates belong to the group of inclusion compounds, in which noncovalent interactions between host and guest substructures play a key role in the arrangement and stabilization of the crystal structure.[1] Sodium silicide Na_8Si_{46}, discovered over 40 years ago,[2] was the first example of an intermetallic compound that can adopt the crystal structure of the type I gas hydrate, also known as the clathrate I structure type. Subsequently, more than 100 type I clathrates of the group 14 elements were synthesized and scrutinized.[3] Their crystal structure is best described as a three-dimensional host framework based on Si, Ge, or Sn trapping cations of alkali, alkaline-earth metals, or europium as guest atoms in the large polyhedral cages. This type of clathrates is known as anionic clathrates or simply clathrates since the negatively charged host framework is balanced by guest cations. The host framework of cationic clathrates or clathrates with inversed host−guest polarity is built of Si, Ge, and Sn and always with an addition of a Group 15 element (pnicogen), tellurium, or even iodine, with halogen or tellurium anions serving as guests. Starting with the preparation of germanium clathrates $Ge_{38}Z_8X_8$ (Z = P, As, or Sb; X = Cl, Br, or I) by von Schnering and Menke,[4] a number of tin[5] and several new germanium[6] cationic type I

* To whom correspondence should be addressed. E-mail: shev@inorg.chem.msu.ru. Fax: (+7-495) 939 47 88.
‡ Max-Planck-Institut für Chemische Physik fester Stoffe.
† Lomonosov Moscow State University.
§ Present address: Department of Chemistry and Biochemistry, Florida State University, Tallahassee, FL, 32306.

(1) Jeffrey G. A. In *Inclusion Compounds*; Atwood, J. L., Davies, J. E. D., MacNicol, D. D., Eds.; Academic Press Inc.: London, 1984.
(2) Kasper, J. S.; Hagenmuller, P.; Pouchard, M.; Cros, C. *Science* **1965**, *150*, 1713–1714.
(3) (a) Kovnir, K. A.; Shevelkov, A. V. *Russ. Chem. Rev.* **2004**, *73*, 923–938, and references therein. (b) Jung, W.; Lörincz, J.; Ramlau, R.; Borrmann, H.; Prots, Y.; Haarmann, F.; Schnelle, W.; Burkhardt, U.; Baitinger, M.; Grin, Y. *Angew. Chem., Int. Ed.* **2007**, *46*, 6725–6728. (c) Condron, C. L.; Kauzlarich, S. M.; Nolas, G. S. *Inorg. Chem.* **2007**, *46*, 2556–2562. (d) Böhme, B.; Guloy, A.; Tang, Z.; Schnelle, W.; Burkhardt, U.; Baitinger, M.; Grin, Y. *J. Am. Chem. Soc.* **2007**, *129*, 5348–5349. (e) Melnychenko-Koblyuk, N.; Grytsiv, A.; Rogl, P.; Rotter, M.; Lackner, R.; Bauer, E.; Fornasari, L.; Marabelli, F.; Giester, G. *Phys. Rev. B* **2007**, *76*, 195124. (f) Kaltzoglou, A.; Ponou, S.; Fässler, T. F. *Eur. J. Inorg. Chem.* **2008**, 538–542.

10.1021/ic8023887 CCC: $40.75
Published on Web 03/12/2009

clathrates were obtained. However, only three silicon-based cationic clathrates have been known up to now: $Si_{40}P_6I_{6.5}$,[7] $Si_{38}Te_{16}$,[8] and $Si_{44.5}I_{1.5}I_8$.[9] The latter two compounds were synthesized under high pressure only.

The electron balance between hosts and guests in cationic and anionic clathrates is achieved by substitution and/or vacancy formation in either host or guest positions, and in many cases the clathrates composition fulfills the 8-*n* rule, thus, the Zintl concept.[10] The interest into the clathrate topic has been renewed owing to the concept phonon glass – electron crystal (PGEC) introduced by Slack.[11] This concept claimed that an advanced material for thermoelectric cooling or power generation would be found among compounds in which guest atoms trapped inside oversized cages are able to rattle. This would lead to a suppression of the thermal conductivity because of effective phonon scattering without impeding the transport of charge carriers. Such a combination of properties would ensure a high figure of merit, $ZT = S^2T\sigma/\kappa$ (T is temperature, σ is electrical conductivity, S is the Seebeck coefficient, and κ is thermal conductivity) of a thermoelectric material.

Our systematic study of cationic clathrates[5a−e,6b,7] had led to the investigation of the ternary system Si−P−Te, which turned out to be a challenge because of various preparative and characterization problems.[12a] Recently, a short communication about thermoelectric properties of a clathrate I with an unspecified composition $Si_{46-x}P_xTe_8$ was published, but no detailed investigation of its composition and crystal structure, in particular phosphorus distribution and homogeneity range, was performed.[12b] We have applied a number of physical and chemical characterization methods to overcome most obstacles and to shed some light on the relationship between the composition, crystal structure, and physical properties for the new cationic clathrate $Si_{46-x}P_xTe_y$ ($6.6(1) \leq y \leq 7.5(1)$, $x \leq 2y$).

Experimental Section

Sample Preparation. Preparation and storage of the samples and the starting materials were carried out in an argon-filled glovebox (content of O_2 <1.2 ppm, H_2O <1 ppm). Silicon (99.9999%, ABCR), red phosphorus (99.995%, Chempur), and tellurium (99.995%, Chempur) were used. Pieces of silicon and tellurium were separately reground in a tungsten carbide mortar and then were sifted (mesh size 0.63 or 0.8 μm). Phosphorus was mechanically pulverized in an agate mortar. Powders of the elements (0.5−2 g total weight) were mixed in respective stoichiometric ratios and were sealed in fused silica ampules (inner diameter 9.5 mm, outer diameter 13 mm, length approximately 60 mm) under vacuum. Samples were synthesized by a two-step annealing. Ampules with the stoichiometric mixtures of the starting materials were placed in furnaces, heated to 1375 K in 24 h, and annealed for 100 h. Afterward, the samples were cooled, ground, and annealed again in fused silica ampules sealed under vacuum at the same temperature for 144 h. Finally, the ampules were cooled to room temperature in the furnace. An additional series of syntheses was performed with the same conditions but with a lower temperature of 925 K.

For neutron powder diffraction studies, the samples (∼5 g) were prepared by either two-step annealing at 1375 K or two-step annealing at 1375/1075 K, but in all cases large fused silica ampules (inner diameter 18.5 mm, outer diameter 19.5 mm, length ≈110 mm) were used. Ampules were placed into a furnace, heated to 1375 K in 24 h, and annealed for 100 h. The samples were reground and annealed in fused silica ampules sealed under vacuum at the same temperature of 1375 K for 144 h (sample 1) or at 1075 K for 120 h (sample 2).

X-ray Powder Diffraction. All samples were analyzed by X-ray powder diffraction in a transmission alignment using a Huber G670 image plate camera, Cu $K\alpha_1$ radiation, $\lambda = 1.540598$ Å. The unit cell parameters were calculated from least-squares fits using LaB_6 (cubic, $a = 4.15692$ Å) as an internal standard utilizing the program package WinCSD.[13] Lattice parameters were obtained from the refinement of a set of 54 reflections common for all samples. Rietveld refinement was performed using the JANA2000 program package.[14]

Scanning Electron Microscopy (SEM) and Wavelength Dispersive X-ray Spectroscopy (WDXS). Selected samples were analyzed by means of SEM. In order to investigate the phase distribution, metallographic studies were performed first. The samples were analyzed by light and electron optical microscopy. The preparation of the samples, including embedding in conductive resin and diamond polishing using dried hexane as a lubricant, was carried out in an inert atmosphere of an argon-filled glovebox.[15] The surface of the samples was further examined in partly polarized light (ZEISS Axioplan2 optical microscope) using differential interference contrast.

(4) (a) von Schnering, H. G.; Menke, H. *Angew. Chem., Int. Ed.* **1972**, *11*, 43–44. (b) Menke, H.; von Schnering, H. G. *Z. Anorg. Allg. Chem.* **1973**, *395*, 223–238.

(5) (a) Shatruk, M. M.; Kovnir, K. A.; Shevelkov, A. V.; Presnyakov, I. A.; Popovkin, B. A. *Inorg. Chem.* **1999**, *38*, 3455–3457. (b) Shatruk, M. M.; Kovnir, K. A.; Lindsjö, M.; Presniakov, I. A.; Kloo, L. A.; Shevelkov, A. V. *J. Solid State Chem.* **2001**, *161*, 233–242. (c) Kovnir, K. A.; Shatruk, M. M.; Reshetova, L. N.; Presniakov, I. A.; Dikarev, E. V.; Baitinger, M.; Haarmann, F.; Schnelle, W.; Baenitz, M.; Grin, Yu.; Shevelkov, A. V. *Solid State Sci.* **2005**, *7*, 957–968. (d) Zaikina, J. V.; Kovnir, K. A.; Sobolev, A. V.; Presniakov, I. A.; Prots, Y.; Baitinger, M.; Schnelle, W.; Olenev, A. V.; Lebedev, O. I.; Van Tendeloo, G.; Grin, Y.; Shevelkov, A. V. *Chem. Eur. J.* **2007**, *13*, 5090–5099. (e) Kovnir, K. A.; Sobolev, A. V.; Presniakov, I. A.; Lebedev, O. I.; Van Tendeloo, G.; Schnelle, W.; Grin, Y.; Shevelkov, A. V. *Inorg. Chem.* **2005**, *44*, 8786–8793. (f) Kishimoto, K.; Arimura, S.; Koyanagi, T. *Appl. Phys. Lett.* **2006**, *88* (1−3), 222115.

(6) (a) Nesper, R.; Curda, J.; von Schnering, H. G. *Angew. Chem., Int. Ed. Engl.* **1986**, *25*, 350–352. (b) Kovnir, K. A.; Abramchuk, N. S.; Zaikina, J. V.; Baitinger, M.; Burkhardt, U.; Schnelle, W.; Olenev, A. V.; Lebedev, O. I.; Van Tendeloo, G.; Dikarev, E. V.; Shevelkov, A. V. *Z. Kristallogr.−New Cryst. Struct.* **2006**, *221*, 527–532. (c) Kishimoto, K.; Akai, K.; Muraoka, N.; Koyanagi, T.; Matsuura, M. *Appl. Phys. Lett.* **2006**, *89* (1−3), 172106.

(7) Kovnir, K. A.; Uglov, A. N.; Zaikina, J. V.; Shevelkov, A. V. *Mendeleev Commun.* **2004**, 135–136.

(8) Jaussaud, N.; Toulemonde, P.; Pouchard, M.; San Miguel, A.; Gravereau, P.; Pechev, S.; Goglio, G.; Cros, C. *Solid State Sci.* **2004**, *6*, 401–411.

(9) Reny, E.; Yamanaka, S.; Cros, C.; Pouchard, M. *Chem. Commun.* **2000**, 2505–2506.

(10) *Chemistry, Structure, and Bonding of Zintl Phases and Ions*; Kauzlarich, M. S., Ed.; VCH Publishers: New York, 1996.

(11) Slack, G. A. In *CRC Handbook of Thermoelectrics;* Rowe, D. M., Ed.; CRC Press LLC: Boca Raton, FL, 1995.

(12) (a) Zaikina, J. V.; Kovnir, K. A.; Demtschyna, R.; Burkhardt, U.; Prots, Y.; Borrmann, H.; Schwarz, U.; Shevelkov, A. V. *Book of Abstracts, The 10th European Conference on Solid State Chemistry* **2005**, *P096*, 162. (b) Kishimoto, K.; Koyanagi, T.; Agai, K.; Matsuura, M. *Jpn. J. Appl. Phys. Part 2* **2007**, *46*, L746−L748.

(13) Akselrud, L. G.; Zavalij, P. Y.; Grin, Yu.; Pecharsky, V. K.; Baumgartner, B.; Wölfel, E. *Mater. Sci. Forum* **1993**, *133−136*, 335–351.

(14) Petricek, V.; Dusek, M.; Palatinus, L. *Jana2000. The Crystallographic Computing System.* Institute of Physics: Praha, Czech Republic, 2000.

(15) Schnelle, W.; Burkhardt, U.; Ramlau, R.; Niewa, R.; Sparn, G. *Scientific Report MPI CPfS* **2003**, 38–43.

Microstructures were homogeneous or showed the majority phase with irregular-shaped grains up to 200 μm. The minority phases in the case of non-single-phase samples were observed in material contrast images collected by the BSE (back-scattered electron) detector of an electron microprobe Cameca SX100 with tungsten cathode.

The composition of the ternary phase was determined by WDXS carried out with the electron microprobe. The intensities of the X-ray lines P K_α, Si K_α, and Te L_α were determined on two wavelength dispersive spectrometers equipped with focusing monochromator crystals made of TAP (thallium acid phthalate) and PET (pentaerythritol). An electron beam current of 10 nA was adjusted for suitable count rates at the acceleration voltages of 25 kV (Te L_α) and 15 kV (P K_α, Si K_α). The signals were compared to the intensities of the reference materials SiP_2 and GeTe.[16] After matrix corrections and averaging over 10 points, an overall value of $\Sigma =$ 100.2(2) wt % was found. The homogeneity and chemical composition of the reference materials were verified by X-ray powder diffraction and chemical analysis, respectively.

Chemical Analysis. Samples for the neutron diffraction experiments and standards for WDXS were characterized by chemical analysis using an inductively coupled plasma optical emission spectrometry method as implemented in a Varian Vista RL spectrometer. For sample dissolution, a microwave-assisted acid digestion (mixture of 3 mL of aqua regia ($HCl:HNO_3$, 3:1) and 0.05 μL of HF) was applied. All values are the average of at least three replicates. The precise determination of composition of the samples in the Si−P−Te system was hampered by the simultaneous presence of volatile (phosphorus and tellurium) and sparingly soluble (silicon) components, which resulted in the inaccurate overall composition deviating from 100%.

Thermal Behavior. Differential scanning calorimetry (DSC) and thermal gravimetric investigations were performed with the Netzsch DSC 409C equipment in a quartz glass crucible sealed under vacuum or in an open quartz crucible (static air), correspondingly, in the temperature range of 300−1550 K with a heating rate of 5 K/min. After cooling with the same rate, the samples were examined by X-ray powder diffraction.

Neutron Powder Diffraction. Neutron powder diffraction patterns of the samples were recorded using the high-resolution powder D2B diffractometer[17] at the Institute Max von Laue-Paul Langevin (Grenoble, France). A polycrystalline sample (~5 g) was placed in a cylindrical vanadium can. The [331] reflection from the Ge monochromator crystal was used to produce a monochromatic neutron beam of wavelength 2.3985 Å. Data were collected at room temperature in a 2θ angular range from 10° to 155° with a step size of 0.05°. The total counting time was approximately 4 h. The raw data were merged using the LAMP program.[18] Diffraction patterns were analyzed by the Rietveld refinement method using the GSAS software package.[19] The only peak belonging to the vanadium can was subtracted. For each sample the profile parameters, background parameters, zero correction, and lattice constant were refined first. The background was fitted using a shifted 14-order Chebyshev polynomial function. A pseudo-Voigt function was applied to generate the profile shape. The following neutron scattering lengths were used: $b_{Te} = 5.80$ fm, $b_P = 5.13$ fm, $b_{Si} = 4.15$ fm.[20]

Physical Property Measurements. The magnetic susceptibility $\chi = M/H$ was measured in external magnetic fields $\mu_0 H$ of 0.01, 0.1, 1, 3.5, and 7.0 T over a temperature range of 1.8−400 K using a MPMS XL-7 SQUID magnetometer (Quantum Design). Rather small polycrystalline samples ($m = 48-87$ mg) were placed in polyethylene tubes and were held in place by short pieces ($m \approx 15$ mg) of the same material. Corrections for the diamagnetism of the individual sample holders were applied.

Electrical resistivity measurements were performed on the same samples with a standard dc (direct current) four-point method between 4 and 320 K. Contacts were made with a silver-filled epoxy paste. Because of the small size of the pieces and resulting problems in the determination of the contact geometry, the inaccuracy of the absolute resistivity is estimated to be ±30%.

All sample handling for physical properties measurements was done under inert atmosphere.

NMR Spectroscopy. ^{31}P magic-angle spinning (MAS) and static wide line (SWL) NMR experiments were done using a Bruker AVANCE spectrometer with $B_0 = 11.74$ T equipped with a standard Bruker MAS probe. The sample was mounted in a 4 mm zirconium dioxide rotor for spinning frequencies below and above 15 kHz. A Hahn echo sequence was used in all experiments with an interpulse delay of 100 μs in SWL and was synchronized with rotor frequency in MAS experiments. The durations for the π-pulses were 3 and 200 μs in nonselective and selective excitation experiments, respectively. A repetition time of 2 s was sufficient to ensure full recovery of the longitudinal magnetization. The signal shift was referred to H_3PO_4.

Results and Discussion

Crystal Structure Description and Comparison with Other Clathrates. The details of the X-ray single-crystal diffraction experiments and a brief crystal structure description of the clathrate I $Si_{46-x}P_xTe_y$ ($y = 7.35, 6.98, 6.88$; $x \leq 2y$) have been already published in our recent short communication.[21] However, it is worthwhile to outline some basic details concerning the atomic arrangement of the title compound. The ideal crystal structure of the clathrate I has the composition G_8E_{46}, where the guest atoms G are enclosed in large cages of the four-connected host framework consisting of 46 E atoms (Figure 1). The framework atoms occupy three crystallographic positions, 6*c*, 16*i*, and 24*k*, of the space group $Pm\bar{3}n$ (no. 223), while the guest atoms reside in the 2*a* and 6*d* positions situated in the center of the 20- and 24-vertex polyhedral cages, respectively, alternating in the unit cell in the 2:6 ratio.

The variations of the ideal G_8E_{46} composition due to the formation of vacancies in either guest positions or host framework in order to achieve the Zintl composition or because of the host−guest matching are described in the literature.[3,5a−d,7] Deviations from the space group $Pm\bar{3}n$ or even superstructure formation resulting in the loss of the cubic symmetry were also observed for several clathrates

(16) (a) Kanatzidis, M. G.; Pöttgen, R.; Jeitschko, W. *Angew. Chem., Int. Ed* **2005**, *44*, 6996–7023. (b) Compound GeTe with the accurately defined composition was donated by Dr. V. I. Shtanov (Chemistry Department, Lomonosov Moscow State University).
(17) High-resolution two-axis diffractometer D2B. 2007. Institut Laue-Langevin, Grenoble, France; http://www.ill.eu/d2b/.
(18) The Large Array Manipulation Program (LAMP); http://www.ill.fr/data_treat/lamp/lamp.html.
(19) (a) Larson, A. C.; Von Dreele, R. B. *General Structure Analysis System (GSAS). Los Alamos National Laboratory Report (LAUR)* **2000**, *86−748*, 1–224. (b) Toby, B. H. *J. Appl. Crystallogr.* **2001**, *34*, 210–213.
(20) Sears, V. *Neutron News* **1992**, *3*, 26–37.
(21) Zaikina, J. V.; Kovnir, K. A.; Schwarz, U.; Borrmann, H.; Shevelkov, A. V. *Z. Kristallogr. – New Cryst. Struct.* **2007**, *222*, 177–179.

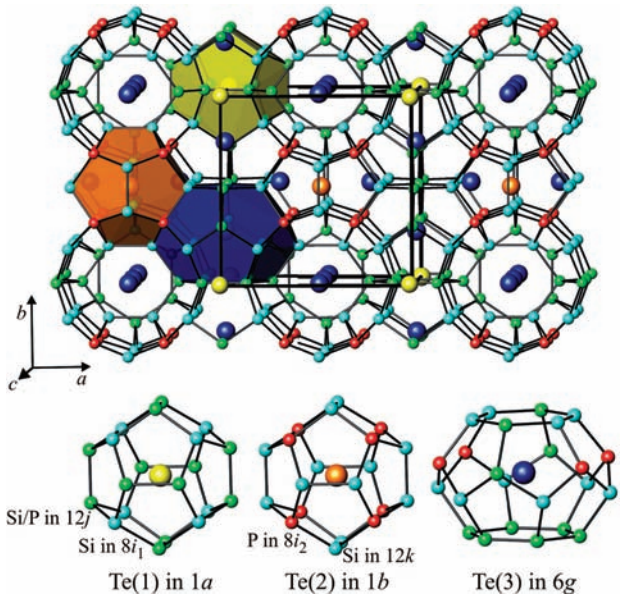

Figure 1. Crystal structure of clathrate I $Si_{46-x}P_xTe_y$. 20-vertex polyhedra for Te(1) and Te(2) and 24-vertex polyhedron for Te(3) are emphasized.

Scheme 1. Wyckoff Site Transformation from the Space Group $Pm\bar{3}n$ to the $Pm\bar{3}$ Space Group for Clathrate I Structure

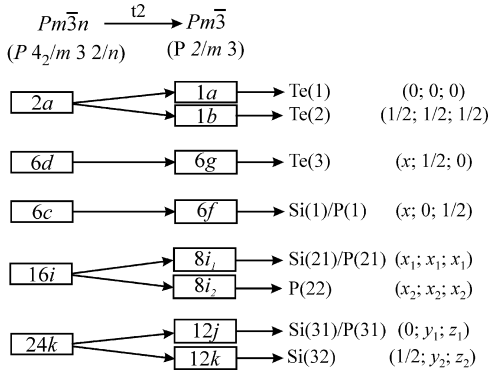

due to either the ordering of vacancies or the separation/ordering of different atoms at distinct framework positions.[3a,4,5b,d,8,22]

The solid solution $Si_{46-x}P_xTe_y$ is a new cationic clathrate I. It crystallizes in space group $Pm\bar{3}$ (no. 200), which is a subgroup of the space group $Pm\bar{3}n$ corresponding to the ideal clathrate I structure type. The host framework is composed of silicon and phosphorus atoms, while tellurium atoms occupy the guest positions. Upon the transformation from the space group $Pm\bar{3}n$ to the space group $Pm\bar{3}$, both guest and framework positions split into crystallographically different sites (Scheme 1). The guest position 2*a* turns into two one-fold positions, 1*a* and 1*b*. The splitting of the framework positions 16*i* and 24*k* of the space group $Pm\bar{3}n$ leads to the positions $8i_1$ and $8i_2$ and 12*j* and 12*k* of the space group $Pm\bar{3}$, correspondingly. The obvious reason for the change of the space group is the vacancy segregation in one of the tellurium guest positions in the center of the 20-vertex cage, 1*b*, while the occupancy of the 1*a* position is always larger. Such a difference in the occupation of the positions 1*a* and 1*b* by tellurium is associated with a difference in their coordination (Figure 1). Each atom, Te(1) or Te(2), is surrounded by 20 framework atoms located in the 8-fold and 12-fold positions. The distances between Te and the atoms in the 8-fold position are relatively short and lie in the range of 3.16−3.19 Å. In the case of a fully occupied Te(1), the 8-fold position is either solely or mainly occupied by silicon, while it is merely occupied by phosphorus atoms in the case of the vacancy-containing Te(2) position. Thus, the symmetry reduction from $Pm\bar{3}n$ to $Pm\bar{3}$ leads not only to a segregation of tellurium vacancies in one of the positions in the center of the 20-vertex polyhedron, but also to the preferred occupation of the polyhedral vertexes by either silicon or phosphorus atoms. Within the framework, the interatomic distances fall in the range of 2.30−2.34 Å, typical for the single covalent bonds Si−Si and Si−P. The distances between the positions that are fully occupied by silicon are slightly larger than those occurring between the positions with a mixed Si/P occupation, while the distances of ∼2.20 Å corresponding to the single covalent P−P bond are not observed in the structure. Such a separation of phosphorus atoms from each other could be an additional reason for the lowering of the symmetry and for the change of the space group from $Pm\bar{3}n$ to $Pm\bar{3}$. This crystal structure model was proposed on the basis of X-ray single-crystal diffraction data with $\sin(\theta)/\lambda > 1$, data/parameters > 50, that allowed to reliably distinguish between the positions occupied exclusively by phosphorus or silicon atoms.

Several examples of clathrates I, all based on silicon, which contain vacancies in the guest positions are known. They are the anionic clathrates $Rb_{6.15(2)}\square_{1.85}Si_{46}$,[23] $K_{8-x}Si_{46}$,[3d,23] superconducting $Ba_{8-x}\square_xSi_{46}$[24] and $Na_xBa_6\square_{2-x}Si_{46}$,[25] and the cationic clathrate $Si_{40}P_6I_{6.5}\square_{1.5}$.[7] The vacancy formation in all these clathrates does not lead to a change/lowering of the symmetry. Thus, to the best of our knowledge, $Si_{46-x}P_xTe_y$ is the first example of a clathrate I compound that exhibits guest vacancy ordering resulting in the change of the space group from $Pm\bar{3}n$ to $Pm\bar{3}$.

Two other examples of cationic clathrates having tellurium as guest atoms, $Si_{38}Te_{16}$[8] and $Ge_{30}P_{16}Te_8$,[6c] were reported recently. The crystal structure of $Si_{38}Te_{16}$, or more precisely $[Si_{38}Te_8]Te_8$, determined by means of X-ray single-crystal diffraction corresponds to the Si−Te host framework trapping Te atoms inside the cages. The authors[8] suggested a change of the space group from $Pm\bar{3}n$ to $P\bar{4}3n$ with the concomitant splitting of the 16-fold position into two 8-fold sites. One of those positions is exclusively occupied by silicon, while another one is filled by tellurium. Tellurium guest atoms were set as fully occupied positions in the center of 20- and 24-vertex cages. However, the reported value of the atomic displacement parameters (ADP) for the Te atom in the smaller 20-vertex cage was almost the same as that refined for the Te atom in the large 24-vertex cage. This most likely

(22) (a) Carrillo-Cabrera, W.; Budnyk, S.; Prots, Y.; Grin, Y. *Z. Anorg. Allg. Chem.* **2004**, *630*, 2267–2276. (b) Dubois, F.; Fässler, T. F. *J. Am. Chem. Soc.* **2005**, *127*, 3264–3265. (c) Dünner, J.; Mewis, A. *Z. Anorg. Allg. Chem.* **1995**, *621*, 191–196.

(23) Ramachandran, G. K.; McMillan, P. F.; Dong, J.; Sankey, O. F. *J. Solid State Chem.* **2000**, *154*, 626–634.

(24) Fukuoka, H.; Kiyoto, J.; Yamanaka, S. *Inorg. Chem.* **2003**, *42*, 2933–2937.

(25) Kawaji, H.; Iwai, K.; Yamanaka, S.; Ishikawa, M. *Solid State Commun.* **1996**, *100*, 393–395.

indicates a partial occupation of the tellurium position in the center of the smaller 20-vertex cage, since usually clathrate I compounds feature almost 2 times larger and anisotropic ADP for the guest atoms in the larger 24-vertex cage compared to the ADP for the guest atom in the smaller cage. Further, the relatively high ADP for silicon in one of the 8-fold positions compared to the other silicon framework atoms may point to the vacancies in this position and, thus, may lead to a deviation from the composition $[Si_{38}Te_8]Te_8$.

The crystal structure and composition of the second tellurium-containing clathrate $Ge_{30}P_{16}Te_8$ were determined by Rietveld refinement of X-ray powder diffraction data.[6c] However, the composition was not confirmed by any additional method. The reported crystal structure of $Ge_{30}P_{16}Te_8$ corresponds to a Ge−P host framework, where phosphorus atoms preferably occupy the 16*i* position of space group $Pm\bar{3}n$, while tellurium atoms serve as guests. On the basis of the X-ray powder data, the authors suggested a partial occupation of 85 and 95% for the tellurium atoms in the center of 20- and 24-vertex cages, respectively. The refined composition corresponds to $[Ge_{30.1}P_{15.9}]Te_{7.4}$ with vacancies in the tellurium guest positions. Homogeneity ranges for the tellurium-containing clathrates $[Si_{38}Te_8]Te_8$ and $[Ge_{30}P_{16}]Te_8$ were not reported.

Synthesis, X-ray Powder Diffraction Data, and Homogeneity Range. As discussed above, $Si_{46-x}P_xTe_y$ shows Te vacancies in the smaller cage. A different number of vacancies and a corresponding different number of tellurium guest atoms cause a broad homogeneity range. We investigated different compositions of the clathrate $Si_{46-x}P_xTe_y$ by means of X-ray powder diffraction.

The starting composition was calculated according to the Zintl concept, assuming that each isolated tellurium guest atom carries a formal charge of −2, while the four-bonded phosphorus atoms of the framework have a formal charge of +1. Further, taking into account that the vacancies are formed in the guest tellurium positions but not in the host framework, the composition $Si_{46-x}P_xTe_y$ ($x = 2y$) could be deduced with a phosphorus content being twice as large as the tellurium amount. Samples with the nominal compositions $Si_{46-x}P_xTe_y$ ($y = 6.3, 6.5, 6.75, 7.00, 7.35, 7.5, 7.75$, $x = 2y$) were synthesized by two-step annealing at 1375 K. The synthesis temperature was chosen just below the decomposition temperature of $Si_{46-x}P_xTe_y$ (~1460 K, see below) and the synthesis temperature of the binary $Si_{38}Te_{16}$ clathrate.[8] However, the formation of the target clathrate phase also occurred at lower temperatures (925 K) similar to the synthesis temperature of $Si_{40}P_6I_{6.5}$,[7] indicating that the formation of the clathrate is also possible via the gas phase without the melting of silicon.

The X-ray powder diffraction data show that the $Si_{46-x}P_xTe_y$ samples with the nominal composition $6.5 \leq y_{nom} \leq 7.5$ correspond to the pure clathrate I phase. The actual tellurium content, *y*, was determined by WDXS analysis, as well as by Rietveld refinement, assuming the composition $Si_{46}Te_y$ taking into account the similarity of the X-ray scattering factors for Si and P. Such a combination of the methods

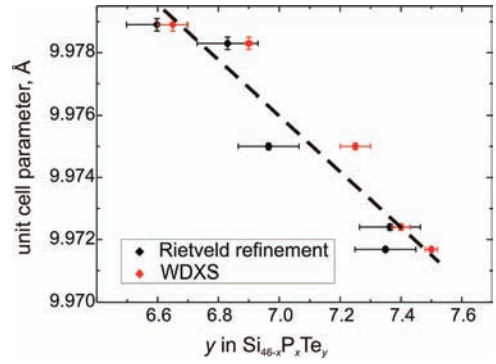

Figure 2. Dependence of the cubic unit cell parameter, *a*, upon Te content, *y*, in $Si_{46-x}P_xTe_y$ determined by Rietveld refinement (black rhombs) and by WDXS (red rhombs). The linear fit is represented by dashed line. The esd's (estimated standard deviation) in determination of the unit cell parameters by powder XRD do not exceed 0.0002 Å, which is smaller than the symbols used. The esd's for the Te content determined by Rietveld refinement are considered to be 0.1 per clathrate formula due to the underestimation of this value given by Rietveld method.

confirmed that the actual tellurium content of the single-phase samples was close to the starting composition (Figure 2). The precise determination of the cubic unit cell parameter of the clathrate I $Si_{46-x}P_xTe_y$ revealed that *a* varied from 9.9789(2) to 9.9724(1) Å, linearly *decreasing with increasing* tellurium content from $y = 6.6(1)$ to $y = 7.5(1)$ (Figure 2).

The samples with the starting composition $y_{nom} < 6.5$ and $y_{nom} > 7.5$ were not single-phase and exhibited no unit cell parameter changes within three esd compared to the corresponding single-phase border compositions. The sample with the nominal composition $y_{nom} > 7.5$ contained impurities of Si_2Te_3 and phosphide SiP_2, while the sample with the low tellurium content ($y_{nom} = 6.3$) constituted a mixture of the clathrate I phase with an impurity of clathrate III $Si_{172-x}P_xTe_y$ ($x = 2y$, $y > 20$).[26]

These findings are compatible with a homogeneity range for the solid solution $Si_{46-x}P_xTe_y$ at 1375 K of $6.5(1) \leq y \leq 7.5(1)$. The linear decrease of the unit cell with increasing tellurium content, *y*, apparently corresponds to an increase of the phosphorus content in $Si_{46-x}P_xTe_y$, $x = 2y$. This is in agreement with the smaller covalent radius of P compared to Si ($r_{cov}(Si) = 1.17$ Å, $r_{cov}(P) = 1.10$ Å),[27] and according to the Zintl concept an increase of the tellurium content necessarily leads to an increase of the phosphorus content. Thus, the increasing amount of Te results in a compression of the Si−P host framework. It should be noted that a combination of the light elements Si and P constituting the host framework leads to the smallest value of the unit cell parameter among all cationic clathrates I and is comparable with that of the anionic clathrate I $K_7B_7Si_{39}$ ($a = 9.952(1)$ Å).[3b]

The change of the space group from $Pm\bar{3}n$ (no. 223), corresponding to the ideal clathrate I structure type, to $Pm\bar{3}$ (no. 200) resulted in the appearance of weak but noticeable reflections with $l \neq 2n$ in the [*hhl*] zone (Figure 3). A complete elimination of these reflections does not occur even

(26) Zaikina, J. V.; Kovnir, K. A.; Haarmann, F.; Schnelle, W.; Burkhardt, U.; Borrmann, H.; Schwarz, U.; Grin, Yu.; Shevelkov, A. V. *Chem. Eur. J.* **2008**, *14*, 5414–5422.
(27) Emsley, J. *The Elements*; Clarendon Press: Oxford, U.K., 1991.

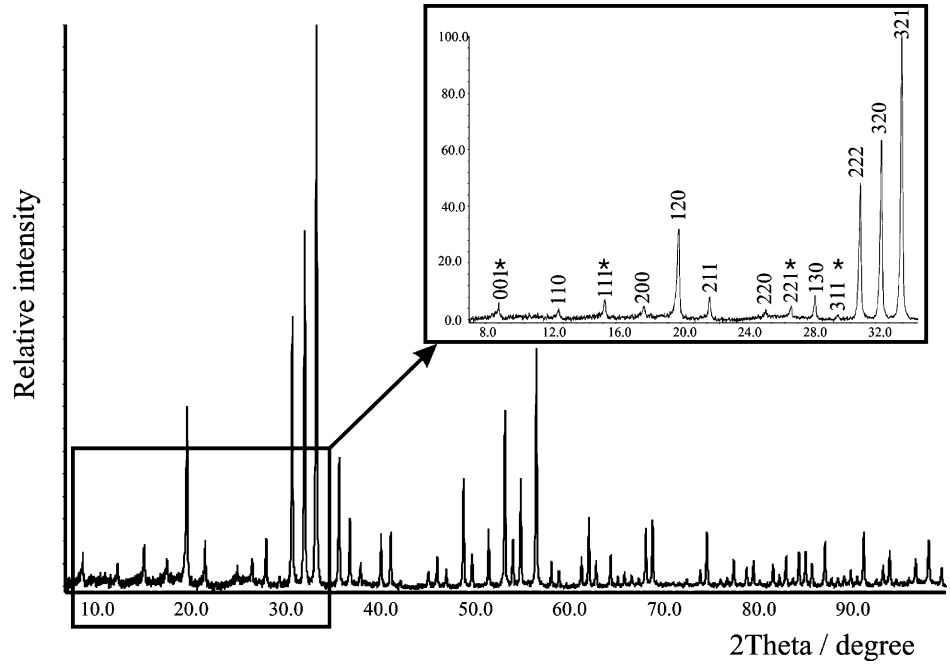

Figure 3. X-ray powder diffraction pattern for $Si_{46-x}P_xTe_y$ with composition $y = 7.25(5)$, $x = 14.10(5)$ (WDXS). The inset shows the representative peaks with $l \neq 2n$ in the [*hhl*] zone marked with asterisk.

for clathrate I phase present in the samples with y_{nom} close to 6 or 8. Calculation of the theoretical X-ray powder diffraction patterns revealed that reflections with $l \neq 2n$ reflected mainly the difference in the occupation of the 1*a* and 1*b* positions. The intensity of these reflections is highest for $y = 7$ when the position 1*a* is fully occupied and the position 1*b* is vacant, and the difference in the occupation is maximal. Thus, $Si_{46-x}P_xTe_y$ always crystallizes at 1375 K in the space group $Pm\bar{3}$ because the difference in occupations of the 1*a* and 1*b* is always present.

SEM, WDXS, and Homogeneity Range. The microstructure images obtained in back-scattering electron (BSE) contrast for the samples $Si_{31.1(1)}P_{14.6(1)}Te_{7.40(3)}$ and $Si_{32.00(5)}P_{14.10(5)}Te_{7.25(5)}$ (WDXS determined) are shown in Figure 4 as a representative example. It is clearly visible that the samples are the single phases. The tellurium content determined by WDXS is in line with that obtained from Rietveld refinement using X-ray powder diffraction data (Figure 2). The P content determined by WDXS is plotted against the Te amount (Figure 5). The ratio x to y in $Si_{46-x}P_xTe_y$ is close to the Zintl composition, $x = 2y$ shown by a solid line. However, the slight but noticeable deviations toward the phosphorus-deficient compositions are evident. Moreover, the increase of the tellurium content is accompanied by an increasing phosphorus amount, which causes a compression of the host framework and a concomitant decrease of the unit cell parameter (Figures 2 and 5).

Neutron Powder Diffraction. Two single-phase clathrate samples (1 and 2) characterized by X-ray powder diffraction, chemical analysis, SEM, and WDXS (Table 1) were used. Crystal structure refinement was performed in the space group $Pm\bar{3}$ (Table 2). After the refinement of the profile parameters, background parameters, zero point correction, and lattice parameter, the atomic coordinates for all the framework positions, as well as for the 6*g* guest position,

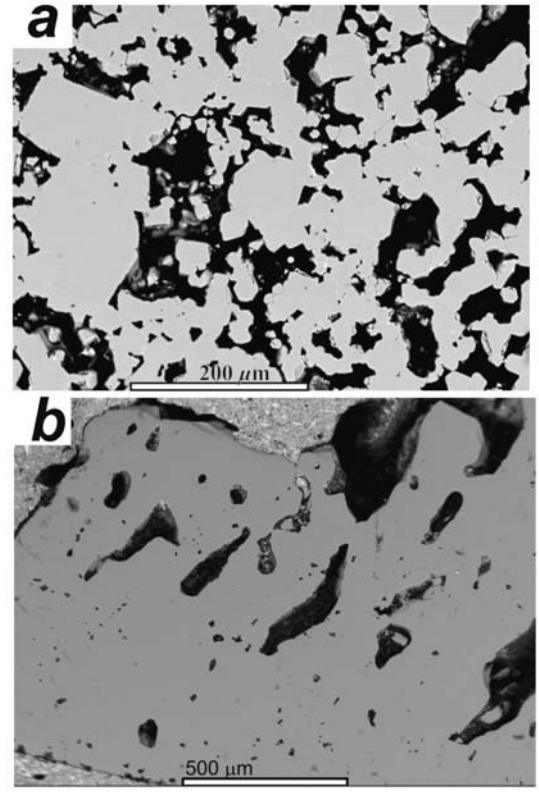

Figure 4. BSE image for (a) $Si_{31.1(1)}P_{14.6(1)}Te_{7.40(3)}$ and (b) $Si_{32.00(5)}P_{14.10(5)}Te_{7.25(5)}$ (composition according to WDXS).

were refined. Each framework position was then set as jointly occupied by silicon and phosphorus. In order to exclude high correlation of the site occupancy factors of the framework positions with mixed Si/P occupations, the total phosphorus amount was fixed to 14.6(1) atoms per unit cell for both samples, which corresponds to the composition determined by the WDXS and chemical analysis. ADPs for all frame-

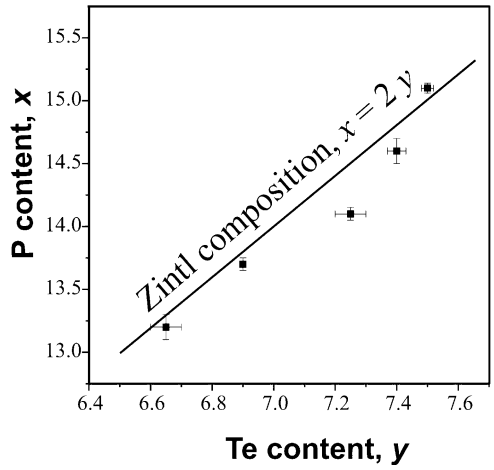

Figure 5. Dependence of the P content upon the Te content in $Si_{46-x}P_xTe_y$ determined by WDXS analysis.

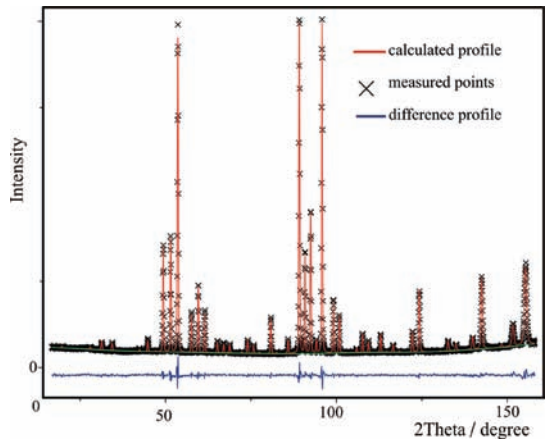

Figure 6. Neutron diffraction Rietveld plot for the refinement of the sample 2, $Si_{31.3}P_{14.7}Te_{7.4}$. Experimental data (points), calculated profile (line), and difference profile (lower part) are shown.

Table 1. Compositions of $Si_{46-x}P_xTe_y$ Samples 1 and 2 Determined by Different Methods

	sample 1	sample 2
unit cell parameter, Å[a]	9.9720(1)	9.9747(1)
WDXS	$Si_{31.3(1)}P_{14.7(1)}Te_{7.45(3)}$	$Si_{31.2(1)}P_{14.8(1)}Te_{7.40(5)}$
chemical analysis	$Si_{30.7(3)}P_{14.7(1)}Te_{7.4(1)}$	$Si_{30.8(2)}P_{14.7(1)}Te_{7.40(3)}$
Rietveld refinement[b]	$Si_{46}Te_{7.3(1)}$	$Si_{46}Te_{7.4(1)}$

[a] X-ray powder data with internal standard. [b] All framework atoms set as Si.

work atoms were constrained to be equal and were isotropically refined. For the Te positions the site occupancy factors and ADPs (anisotropic for 6*g*, isotropic and constrained to be equal for 1*a* and 1*b*) were allowed to vary in a separate series of the structure refinement.

The final refinement revealed that the Te position 1*b* is partly occupied while the Te positions 6*g* and 1*a* remain fully occupied within 1esd. The resulting Si to P distribution is similar to that determined by the X-ray single-crystal refinement.[21] In particular, the $8i_1$ position, which builds up the cage around the tellurium 1*a* position, is preferentially occupied by silicon while the $8i_2$ position, which is next to the vacancy-containing 1*b* Te position, is populated by phosphorus exclusively (Table 3 and Figure 1). Likewise, there is a distinct difference in the 12-fold positions occupancy where silicon exclusively occupies the 12*k* position

Table 2. Data Collection and Structure Refinement Parameters for Crystal Structure Determination Experiments from Neutron Powder Diffraction Data[a]

	sample 1	sample 2
refined composition	$Si_{31.3}P_{14.7}Te_{7.3(2)}$	$Si_{31.3}P_{14.7}Te_{7.4(1)}$
diffractometer	D2B	
temperature, K	295(2) K	
wavelength, λ, Å	2.3985	
range 2θ, degree	10−155	
step size 2θ, degree	0.05	
space group	$Pm\bar{3}$ (*no.* 200)	
lattice parameter, *a*, Å[b]	9.978(1)	9.976(4)
profile *R* factor (R_p)	3.2	3.1
weighted profile *R* factor (R_{wp})	4.1	3.9
structure *R* factor (R_{F2})	4.0	2.5
χ^2	1.99	1.88
profile function	pseudo-Voigt	
background function	14 coefficients shifted Chebyshev function	

[a] The esd in the Rietveld method is usually underestimated.[34] To get more reliable values the following equation was used: $esd_{new} = esd_{Rietveld} N_{points}/N_{hkl}$. [b] The parameters are taken from Rietveld refinement. Those which are determined on the basis of X-ray powder data with internal standard are shown above in Table 1.

Table 3. Crystallographic Data for the $Si_{46-x}P_xTe_y$ Samples 1 and 2[a]; space group $Pm\bar{3}$

	sample 1	sample 2	X-ray single-crystal data[21]
Guest Atoms			
sof Te in 1*a* (0,0,0)	0.9(1)	1	1
sof Te in 1*b* (1/2,1/2,1/2)	0.4(1)	0.4(1)	0.347(2)
U^{iso} Te in 1*a* = 1*b*	0.003(1)	0.011(2)	0.00658(2)/ 0.00727(9)
U^{eq} Te in 6*g* (x,1/2,0)	0.018(1)	0.017(1)	0.01249(1)
Host Framework			
sof Si/P			
6*f*	0.685/0.315(5)	0.70/0.30(2)	0.61/0.39(4)
$8i_1$	0.920/0.080(6)	0.90/0.10(1)	0.89/0.11(3)
$8i_2$	0/1	0/1	0/1
12*j*	0.667/0.333(2)	0.67/0.33(1)	0.71/0.29(2)
12*k*	1/0	1/0	1/0
U^{iso} of Si/P	0.006(1)	0.004(1)	0.0069(7)[b]

[a] The esd in the Rietveld method is usually underestimated.[34] To get more reliable values the following equation was used: $esd_{new} = esd_{Rietveld} N_{points}/N_{hkl}$. [b] Averaged U^{iso} is given.

and preferentially populates the 12*j* position. It should be noted that low intensity of reflections with $l \neq 2n$ in the *hkl* zone defining the transition from the space group $Pm\bar{3}n$ to the space group $Pm\bar{3}$ led to a rather inaccurate determination of the atomic occupancies.

Summing up, the distribution of silicon and phosphorus atoms within the framework, as well as the vacancies at the Te site as refined using neutron powder diffraction data, is in qualitative accordance with the crystal structure model suggested on the basis of the X-ray single-crystal data measured up to high $\sin(\theta)/\lambda$ values.

NMR Spectroscopy. To study different environments of the atoms locally, ^{31}P solid-state NMR experiments for the single-phase sample with the $Si_{32.5(5)}P_{13.2(1)}Te_{6.65(5)}$ composition (determined by WDXS) were performed. The featureless asymmetric line shape of the signal did not change upon magic-angle spinning (Figure 7, top). This evidenced that the signal is composed of shift distributions resulting from minute changes in the local environment, thus causing a variation of the spectral parameters (e.g., isotropic shift, shift

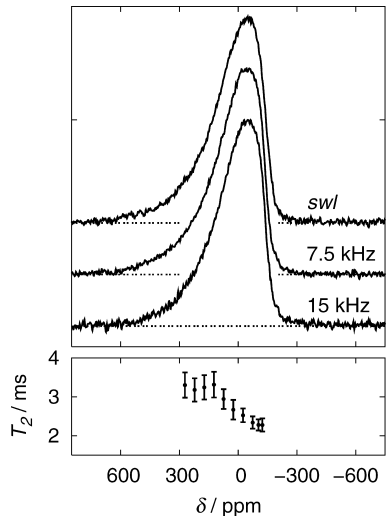

Figure 7. ^{31}P NMR signals of $Si_{32.5}P_{13.2}Te_{6.6}$ measured at ambient temperature and $B_0 = 11.74$ T. The SWL and MAS signals with rotation frequencies of 7.5 and 15 kHz are normalized and separated by an arbitrary offset (top). Spin−spin relaxation time T_2 was obtained from frequency-dependent selective excitation experiments (bottom).

anisotropy, or asymmetry). The distribution of shifts is a characteristic feature for disordered compounds and is frequently observed, for instance, in glasses where the first coordination sphere determines the center of gravity of the NMR signal. The local disorder in the second and higher coordination spheres causes the broadening of the signal.[28] In clathrates, the mechanism causing the broadening of the signal contributions seems to be similar. The signal shift of the center of gravity of the individual signal contributions stems from the next-neighbor coordination. The broadening results from substitutional disorder and/or partially vacant sites in the cages and/or the framework. In the investigated sample $Si_{32.5(5)}P_{13.2(1)}Te_{6.65(5)}$, the vacancies in the framework can be excluded, leaving only substitutional disorder in the framework and partially vacant sites in the small cages as the origin for the broadening of the ^{31}P NMR signal.

The frequency range of the NMR signal of $Si_{32.5(5)}P_{13.2(1)}Te_{6.65(5)}$ (from −300 to 600 ppm) is typically observed for chemical shielding in nonconducting diamagnetic compounds (−400 to 600 ppm).[29] This indicates that the signal shift is only slightly influenced by the interaction of the P nuclei with the conduction electrons; in other words because of the low concentration of charge carriers, the Knight shift is far from being dominant.

The frequency distribution is significantly larger than that in other cationic type I clathrates $Sn_{17}Zn_7P_{22}X_8$ with X = Br, I (from 100 to 230 ppm)[5c] and type III clathrates $Si_{172-x}P_xTe_y$ (−300 to 200 ppm).[26] The ^{31}P NMR signal of sample $Si_{30}P_{16}Te_8$[30] prepared by chemical transport at significantly lower temperatures (800 K) covers a much smaller frequency range ($-250 \leq \delta \leq 150$ ppm). We attribute a much broader frequency range for $Si_{32.5(5)}P_{13.2(1)}Te_{6.65(5)}$ to the large amount of disorder present in the title compound. All findings indicate that the disorder in the latter clathrate is significantly

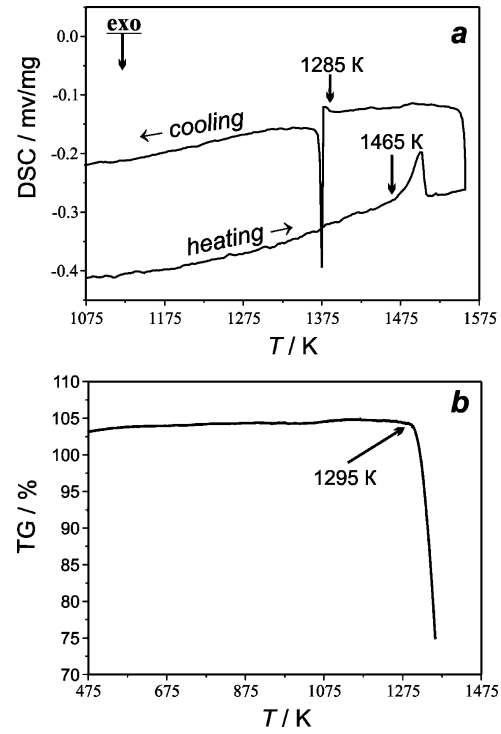

Figure 8. Thermal behavior of clathrate I $Si_{46-x}P_xTe_y$ for (a) DSC experiment in evacuated sealed quartz ampule for the sample $Si_{32.30(5)}P_{13.70(5)}Te_{6.90(1)}$, and (b) TG experiment in open quartz crucible in static air atmosphere for the sample $Si_{32.7(1)}P_{13.3(1)}Te_{6.70(5)}$.

enhanced in comparison to $Si_{30}P_{16}Te_8$.

According to the X-ray single-crystal determination,[21] the estimated ratio of the signal components is 1.4:3.8:8; however, the individual signal contributions could not be resolved. Therefore, evidence for different P sites in $Si_{32.5(5)}P_{13.2(1)}Te_{6.65(5)}$ is obtained by spin−spin relaxation experiments. These are sensitive to the local environment of the nuclei since the homonuclear dipole−dipole coupling can be reduced to extracted signal contributions by the application of the selective excitation. The spin−spin relaxation time T_2 increases by a factor of 2−4 upon the application of selective excitation compared to nonselective excitation and shows characteristic frequency dependence (Figure 7, bottom). The low values indicate small average distances of the interacting spins as observed at low frequency. The high values observed at large frequencies point out a larger average distance of the interacting nuclei. This can be expected for the P atoms neighboring a partially filled small cage, indicating that the signal broadening is influenced by the change of the local environment. The change from low to high values of T_2 is due to the varying amount of the different signal contributions. The crystal structure analysis reveals that the phosphorus atoms tend to avoid each other within the framework.

Thermal Behavior. A typical result of a DSC experiment is shown in Figure 8 for the sample with the compostion $Si_{32.30(5)}P_{13.80(5)}Te_{6.95(1)}$. Analysis of the data (Table 4) revealed changes of the unit cell parameters after the DSC experiment, as well as the presence of admixtures, together with traces of Si_2Te_3 and white phosphorus on top of the DSC ampule. All this indicates that $Si_{46-x}P_xTe_y$ partially decomposes in

(28) Zhang, P.; Dunlap, C.; Florian, P.; Grandinetti, P. J.; Farnan, I.; Stebbins, J. F. *J. Non-Cryst. Solids* **1996**, *204*, 294–300.
(29) *Multinuclear NMR*; Mason, I., Ed.; Plenum Press: New York, 1987.
(30) Philipp, F.; Schmidt, P. *J. Cryst. Growth* **2008**, *310*, 5402–5408.

Table 4. Results of XRD, DSC, and WDXS for the Samples $Si_{46-x}P_xTe_y$ from Homogeneity Range

composition according to WDXS	unit cell parameter, a/Å: before DSC	unit cell parameter, a/Å: after DSC	endothermic effect temperature, K	phase content after DSC
		experiments in sealed under vacuum quartz ampule		
$Si_{32.5(5)}P_{13.2(1)}Te_{6.65(5)}$	9.9789(2)	9.9878(2)	1493	clathrate I, clathrate III[a]
$Si_{32.30(5)}P_{13.80(5)}Te_{6.95(1)}$	9.9783(2)	9.9726(1)	1465	clathrate I, Si, SiP_2
$Si_{32.00(5)}P_{14.10(5)}Te_{7.25(5)}$	9.9750(1)	9.9838(2)	1453	clathrate I, Si_2Te_3
$Si_{31.1(1)}P_{14.6(1)}Te_{7.40(3)}$	9.97168(8)	9.9783(2)	1445	clathrate I, Si_2Te_3
$Si_{30.80(5)}P_{15.10(4)}Te_{7.50(2)}$	9.9724(1)	9.9798(2)	1479	clathrate I, Si_2Te_3
		experiment in open quartz crucible in static air atmosphere		
$Si_{32.5(5)}P_{13.2(1)}Te_{6.65(5)}$	9.9789(2)	9.9787(1)	1295	clathrate I Si, SiO_2[b]

[a] Clathrate III $Si_{172}P_xTe_y$[26] crystallizes in $P4_2/mnm$ space group with unit cell parameters $a = 19.2304(3)$ Å and $c = 10.0602(3)$ Å. [b] Cristobalite.

vacuum. Increasing the unit cell parameter for the samples after DSC clearly demonstrates that $Si_{46-x}P_xTe_y$ becomes tellurium and phosphorus depleted during the DSC experiment. Apparently upon heating, the most volatile clathrate components — tellurium and phosphorus — tend to evaporate, thus shifting the composition of the $Si_{46-x}P_xTe_y$ clathrate I phase along the $x \cong 2y$ line toward a higher silicon content. The sample $Si_{32.5(5)}P_{13.2(1)}Te_{6.65(5)}$ is close to the Te-poorest border composition according to the established homogeneity range of $Si_{46-x}P_xTe_y$. Upon heating in vacuum, it loses tellurium and rearranges with the formation of clathrate III $Si_{172-x}P_xTe_y$.[26] The composition of the clathrate III exhibits a higher Si/Te ratio but is still situated on the line $x = 2y$. Such thermal behavior of clathrate I $Si_{46-x}P_xTe_y$ is similar to that of binary alkali-metal silicides M_4Si_4 (M = Na, K, or Rb). Upon heating, M_4Si_4 loses some amount of alkali-metal leading to a structural rearrangement by forming either clathrate I M_xSi_{46} ($x \leq 8$) or clathrate II M_xSi_{136} ($x \leq 24$).[2,3d,23,31]

Heating of the samples in open crucibles in static air atmosphere showed that $Si_{46-x}P_xTe_y$ is stable up to 1295 K (Figure 8b). Further heating leads to the decomposition of the clathrate I phase with the evaporation of tellurium and phosphorus (Table 4). Clathrate III $Si_{172-x}P_xTe_y$ exhibits an even higher thermal stability in air since it shows no sign of decomposition or oxidation below 1500 K.[26] Therefore, the Si−P−Te clathrates may serve as a basis for the creation of new clathrate-based materials for high-temperature applications.

Electrical Resistivity and Magnetic Properties. $Si_{46-x}P_xTe_y$ samples exhibit different temperature behavior of the electrical conductivity depending on their composition (Figure 9). A typical behavior for thermally activated semiconductors was observed only for $Si_{30.80(5)}P_{15.10(4)}Te_{7.50(2)}$. The value of the band gap $E_g = 0.12$ eV was calculated from linear fits to the corresponding dependence of $\ln(1/\rho)$ upon $1/T$. In turn, the samples with the compositions $Si_{32.5(5)}P_{13.2(1)}Te_{6.65(5)}$ and $Si_{32.00(5)}P_{14.10(5)}Te_{7.25(5)}$ demonstrate temperature dependences of conductivity typical for heavily doped semiconductors, which may be caused either by slight deviation from the Zintl ($x = 2y$) composition or by closing the gap originating from band broadening due to, e.g., stronger disorder.

The high-field magnetic susceptibilities $\chi(T,H) = M/H$ of

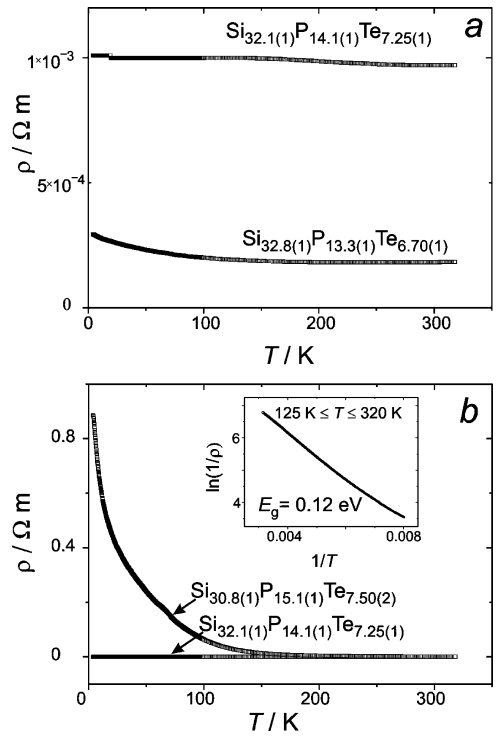

Figure 9. Electrical resistivity vs temperature for $Si_{46-x}P_xTe_y$. Inset: $\ln(1/\rho)$ vs $1/T$ of $Si_{30.8(1)}P_{15.3(1)}Te_{7.50(2)}$.

$Si_{46-x}P_xTe_y$ are weakly field dependent in the whole temperature range. This is due to traces of ferromagnetic impurities with $T_C \gg 400$ K probably originating from steel tools used during the sample preparation and mounting. An extrapolation of $\chi(T,H)$ for $1/H \rightarrow 0$ for high fields (Honda−Owen method[32]) yields corrected values $\chi(T)$ for the susceptibility (Figure 10). Traces of Curie-paramagnetic impurities and possibly paramagnetic point defects (vacancies and structural disorder) lead to the observed upturns in $\chi(T)$ toward low temperatures.

The corrected susceptibility can be written as $\chi(T) = \chi_{dia} + \chi_{struct}(T) + \chi_C(T)$. Here, χ_{dia} is the diamagnetism of the closed-shell ions, which can be calculated as the sum of the diamagnetic increments.[32] It has to be remarked that the latter values have most often been determined from room-temperature measurements ($T \approx 300$ K). $\chi_{struct}(T)$ is a possible "structural increment" caused by molecular ring currents on

(31) Reny, E.; Gravereau, P.; Cros, C.; Pouchard, M. *J. Mater. Chem.* **1998**, *8*, 2839–2844.

(32) Selwood, P. W. *Magnetochemistry*, 2nd ed.; Interscience: New York, 1956.

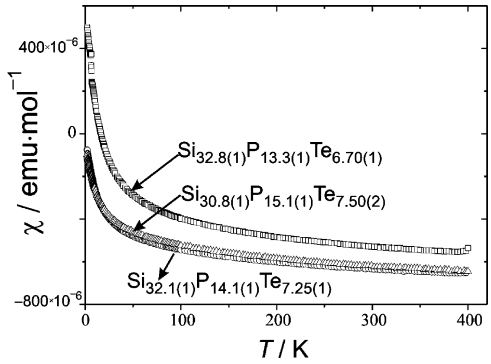

Figure 10. Temperature dependences of the magnetic susceptibility for $Si_{46-x}P_xTe_y$ samples corrected by the Honda−Owen method.

Table 5. Components of Magnetic Susceptibility for $Si_{46-x}P_xTe_y$ at 300 K in emu mol^{-1}[a]

composition[b]	χ_{dia}, emu mol^{-1}	χ_{struct}, emu mol^{-1}	χ_C, emu mol^{-1}
$Si_{32.5(5)}P_{13.2(1)}Te_{6.65(5)}$	-515×10^{-6}	-45×10^{-6}	550×10^{-6}
$Si_{32.00(5)}P_{14.10(5)}Te_{7.25(5)}$	-554×10^{-6}	-96×10^{-6}	310×10^{-6}
$Si_{30.80(5)}P_{15.10(4)}Te_{7.50(2)}$	-571×10^{-6}	-69×10^{-6}	310×10^{-6}

[a] See text for details. [b] Composition is given according to the WDXS data.

the cage walls in the clathrate structure[33] plus other intrinsic contributions. The observed weak linear-in-temperature contribution to $\chi(T)$ is, therefore, included in this $\chi_{struct}(T)$ term. The last term $\chi_C(T)$ represents the above-mentioned impurity and defect contributions, which can be modeled by a Curie law $\chi_C = C/T$. From least-squares fits in the temperature range of 50−400 K, the values for $\chi_0(300\ K) = \chi_{dia} + \chi_{struct}(300\ K)$ and equivalent fractions χ_C of magnetic species with $S = 1/2$ (calculated from the Curie constant C) are calculated, and the values for all three terms are given in Table 5. The resulting values for $\chi_{struct}(300\ K)$ are negative and rather small, on average $-70 \pm 30 \times 10^{-6}$ emu/mol. For clathrates, the absolute values of the structural increment are usually significantly higher, $\approx -300 \times 10^{-6}$ emu/mol for the clathrate I compounds.[32] For the clathrate III $Si_{172-x}P_xTe_y$ with a Si−P framework and Te anions situated in part of the cages, χ_{struct} is -700×10^{-6} emu/mol.[26] The clathrate III structure has 30 cavities per formula unit compared to eight cavities per formula unit in the clathrate I. A value of χ_{struct} for $Si_{172-x}P_xTe_y$ normalized for eight cages is still -200×10^{-6} emu/mol. Therefore, other intrinsic paramagnetic contributions to χ_{struct} may, thus, play an important role in clathrate I $Si_{46-x}P_xTe_y$. Together with the pronounced temperature dependence of the magnetic susceptibility in the whole temperature range, it points out that $Si_{46-x}P_xTe_y$ is not a typical Zintl phase.

Similar properties were observed for a large crystal ($1.5 \times 2.55 \times 0.7$ mm) with the composition $Si_{30.7(1)}P_{15.2(1)}Te_{7.55(3)}$ selected from sample 2 (Figure 11). According to metallographic, SEM, and WDXS studies, the crystal does not

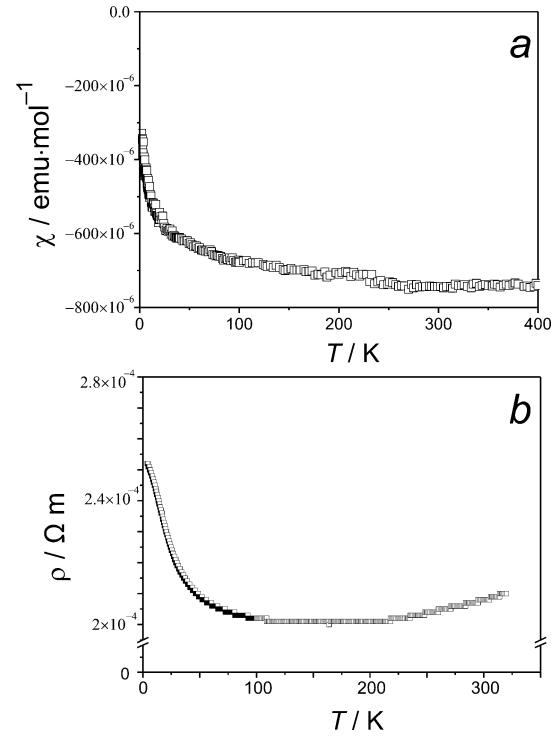

Figure 11. Temperature dependences of electrical resistivity and magnetic susceptibility ($H = 7$ T) of crystal $Si_{30.7(1)}P_{15.2(1)}Te_{7.55(3)}$ (sample 2).

exhibit variation in the composition and does not contain admixtures. The magnetic susceptibility of the investigated crystal is temperature-dependent, with the room-temperature value being $\chi_0(300\ K) = -700(100) \times 10^{-6}$ emu/mol, which is in good agreement with the behavior of the polycrystalline samples. Large standard deviations stem from the small mass of the crystal. The electrical resistivity is typical for heavily doped semiconductors. Investigation of the thermoelectric properties of $Si_{46-x}P_xTe_y$, including the high-temperature region, is currently in progress.

Conclusions

The new cationic clathrate I $Si_{46-x}P_xTe_y$ is synthesized from the elements. It features very high stability (up to 1460 K in vacuum and 1295 K in air), and its cubic unit cell parameter is one of the smallest among clathrates. The presence of vacancies in the guest positions leads to the wide homogeneity range $6.6(1) \le y \le 7.5(1)$, $x \le 2y$ at 1375 K. Vacancies order in one of the 20-vertex cages of the clathrate framework that corresponds to a preferential coordination of guest Te atoms by silicon atoms. Te atoms tend to avoid cages rich in phosphorus, which results in a change of the space group from $Pm\bar{3}n$ (ideal clathrate I structure type) to $Pm\bar{3}$. The presence of the sites with different coordination of phosphorus atoms was confirmed by neutron powder diffraction and ^{31}P NMR spectroscopy. The compositional deviation ($x \le 2y$) from the Zintl concept ($x = 2y$) leads to the properties alien to the Zintl phase − the samples are heavily doped semiconductors and temperature-dependent diamagnets.

Acknowledgment. Authors wish to express their gratitude to Dr. J. Hunger and Dr. E. Suard (Institute Laue-Langevin,

(33) (a) Cros, C.; Pouchard, M.; Hagenmuller, P. *J. Solid State Chem.* **1970**, *2*, 570–581. (b) Paschen, S.; Tran, V. H.; Baenitz, M.; Carrillo-Cabrera, W.; Grin, Y.; Steglich, F. *Phys. Rev. B* **2002**, *65* (1−9), 134435. (c) Zaikina, J. V.; Schnelle, W.; Kovnir, K. A.; Olenev, A. V.; Grin, Y.; Shevelkov, A. V. *Solid State Sci.* **2007**, *9*, 664–671.

(34) (a) Sakata, M.; Cooper, M. J. *J. Appl. Crystallogr.* **1979**, *12*, 554–563. (b) Berar, J.-F; Lelan, P. *J. Appl. Crystallogr.* **1991**, *24*, 1–5.

Grenoble, France) for their help in collecting and refinement of the neutron data, Mr. T. Vogel and Ms. M. Eckert for the metallographic and WDXS investigations, Dr. G. Auffermann and Ms. A. Völzke for the chemical analysis, Dr. V. I. Shtanov for donating a sample of GeTe, and Mr. R. Koban for the measurement of physical properties. J.V.Z. thanks the Max-Planck Society for a research fellowship. This research is supported in part by the Russian Foundation for Basic Research.

Supporting Information Available: A CIF file containing information on two structural experiments. This material is available free of charge via the Internet at http://pubs.acs.org.

IC8023887